Journal Pre-proof

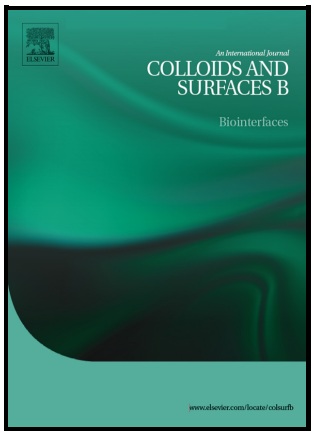

Biocompatibility Characterization of Vaterite with a Bacterial Whole-Cell Biosensor

Dorin Harpaz, Hani Barhom, Boris Veltman, Pavel Ginzburg, Evgeni Eltzov

PII: S0927-7765(22)00788-3

DOI: https://doi.org/10.1016/j.colsurfb.2022.113104

Reference: COLSUB113104

To appear in: *Colloids and Surfaces B: Biointerfaces*

Received date: 15 September 2022
Revised date: 28 November 2022
Accepted date: 14 December 2022

Please cite this article as: Dorin Harpaz, Hani Barhom, Boris Veltman, Pavel Ginzburg and Evgeni Eltzov, Biocompatibility Characterization of Vaterite with a Bacterial Whole-Cell Biosensor, *Colloids and Surfaces B: Biointerfaces,* (2022) doi:https://doi.org/10.1016/j.colsurfb.2022.113104

Biocompatibility Characterization of Vaterite with a Bacterial Whole-Cell Biosensor

Dorin Harpaz [a, b, 1], Hani Barhom [c, 1], Boris Veltman [a, b, 1], Pavel Ginzburg [c] and Evgeni Eltzov [a, d *]

[a] *Institute of Postharvest and Food Science, Department of Postharvest Science, Volcani Institute, Agricultural Research Organization, Rishon LeZion 7505101, Israel; dorin.harpaz@mail.huji.ac.il*

[b] *Institute of Biochemistry, Food Science and Nutrition, Faculty of Agriculture, Food and Environment, The Hebrew University of Jerusalem, Rehovot 76100, Israel; boris.veltman@mail.huji.ac.il*

[c] *School of Electrical Engineering, Tel Aviv University, Tel Aviv 69978, Israel; hanibarhum@mail.tau.ac.il*

[d] *Agro-Nanotechnology and Advanced Materials Research Center, Volcani Institute, Agricultural Research Organization, Rishon LeZion 7505101, Israel*

[1] *These authors contributed equally to this work*

* *Co-corresponding authors: eltzov@volcani.agri.gov.il; +972-3-968-3607 (Evgeni Eltzov) and pginzburg@tauex.tau.ac.il; +972-3-640-6058 (Pavel Ginzburg)*

Abstract

The growing biomedical challenges impose the continuous development of novel platforms. Ensuring the biocompatibility of drug delivery and implantable biomedical devices is an essential requirement. Calcium carbonate ($CaCO_3$) in the form of vaterite nanoparticles is a promising platform, which has demonstrated distinctive optical and biochemical properties, including high porosity and metastability. In this study, the biocompatibility of differently shaped $CaCO_3$ vaterite particles (toroids, ellipsoids, and spheroids) are evaluated by bacterial toxicity mode-of-action with a whole-cell biosensor. Different *Escherichia coli* (*E. coli*) strains were used in the bioluminescent assay, including cytotoxicity, genotoxicity and quorum-sensing. Firstly, both scanning electron microscopy (SEM) and fluorescence microscopy characterizations were conducted. Bacterial cell death and aggregates were observed only in the highest tested concentration of the vaterite particles, especially in toroids *15-25μm*. After, the bioluminescent bacterial panel was exposed to the vaterite particles, and their bioluminescent signal reflected their toxicity mode-of-action. The vaterite particles resulted in an induction factor (IF > 1) on the bacterial panel, which was higher after exposure to the toroids (1.557 ≤ IF ≤ 2.271) and ellipsoids particles (1.712 ≤ IF ≤ 2.018), as compared to the spheroids particles (1.134 ≤ IF ≤ 1.494), in all the tested bacterial strains. Furthermore, the vaterite particles did not affect the viability of the bacterial cells. The bacterial monitoring demonstrated the biofriendly nature of especially spheroids vaterite nanoparticles.

Keywords: vaterite biocompatibility; calcium carbonate ($CaCO_3$); whole-cell biosensor; toxicity mode-of-action; bioluminescence bioreporter bacteria; genotoxicity cytotoxicity quorum-sensing stress.

1. **Introduction**

The expanding biomedical challenges of modern medicine produce continuous developments of novel materials, physical processes, and functional platforms. Particularly, in drug delivery applications, the design of micro- and nanocarriers provides various advantages as compared to conventional injection, macroscopic polymer, or lipid carriers [1]. Efficient carriers encompass biocompatibility, as well as high loading capacity [2]. The biocompatibility of the utilized materials is the main challenge in fields such as drug delivery and implantable biomedical devices [3]. While biogenic materials often do not possess the needed features that are required for the devices performance [4]. Over the past years, inorganic complete the organic need, and inorganic nanoparticles are increasingly used in various theranostic applications [5]. Calcium carbonate ($CaCO_3$) is explored as a

multifunctional platform, capable of accommodating several functionalities simultaneously. Generally, calcium carbonates also contribute to reducing carbon dioxide emission [6], the formation of sediments and rocks [7], elements in leaves [8], as well as global climate change [9, 10]; therefore, $CaCO_3$ is a fundamental research focus worldwide.

Specifically, $CaCO_3$ in a form of vaterite is integrated as a biocompatible drug carrier in various biophotonic applications [11] (e.g., photothermal therapy [12, 13], photoacoustic tomography [14], and bioimaging), and in tissue engineering [15-20]. Vaterite is a metastable polymorph of $CaCO_3$ that was named after the German mineralogist Heinrich Vater in 1911, which seemed to synthesize it as early as 1894. Vaterite has demonstrated distinctive tunable optical and biochemical properties, including high porosity and metastability, which increases its utilization in various applications [21]. The low-cost self-assembly synthesis of vaterite, which is also simple to perform [22], contributes to its frequent usage [23]. The vaterite monocrystals can self-assemble naturally in polycrystal micro- and nanoparticles, which are termed spherulites. Their high porosity enables a high payload capacity [24]. For example, a recent study by the research group reported that polycrystalline sub-micrometer vaterite spherulites demonstrated a volumetric filling ratio exceeding 28% [13].

Vaterite is mostly found in calcareous sediments in nature [25]. While its most natural occurrences are associated with biogenic activity (e.g. calcified tissues (gastropod shells [26]), mollusk pearls [27], gallstones [28, 29], pancreatic stones [30], human heart valves [30], green turtle eggshells [31], crustacean statoliths [32] and fish otoliths [33]) [34]. Still, the most prevalent carbonates are calcite and aragonite [35]. The geometrical (i.e., size and shape) and surface (i.e., charge and hydrophilicity) properties of the $CaCO_3$ particles are influenced by the ratios of the initial salts used in their synthesis [36]. The formation and stabilization of vaterite are aided by the presence of living organisms and even favored as compared to calcite and aragonite [37, 38]. The precipitation of vaterite is induced by various organic polymeric substances such as carboxylic groups [39], phosphonates [40], sulfonates [41], amino acids [42-44], and anionic surfactants [45]. Vaterite usually appears as micron-sized spherulites when it is precipitated in the presence of bacteria [46]. A further understanding of the micro- and nano-structure of vaterite may contribute to its application in various fields [22, 47]. While, biocompatibility is a basic feature to be fully explored to justify the main established use of vaterite (i.e., drug delivery). The biocompatibility of vaterite is continuously and thoroughly explored over the past years, mainly by using various human cell lines [16, 17, 48-54].

In this study, the biocompatibility of differently shaped $CaCO_3$ vaterite particles (toroids, ellipsoids, and spheroids) are estimated by bacterial toxicity mode-of-action with a whole-cell

biosensor. The whole-cell biosensor integrates the bacterial cells that are genetically modified to produce light with a transducer for signal measurement. Different *Escherichia coli* (*E. coli*) strains were used in the bioluminescent assay, including cytotoxicity (TV1061), genotoxicity (DPD2794), and quorum-sensing (K802NR). Also, the biological activity can be monitored by the analysis of viability, gene expression, and metabolic activity [55, 56]. The light signal change of the bacterial cells after exposure to the vaterite particles reflects their toxicity mode-of-action. The whole-cell biosensor was previously tested for the presence of specific chemicals [57-59] or general stresses [60-65]. This approach of bacterial monitoring identifies signatures of the toxicity mode-of-action. To the best of our knowledge, this is the first study to investigate the biocompatibility interaction of bacteria with $CaCO_3$ nanoparticles, while most previous studies investigated the contribution of bacteria to the precipitation of vaterite.

2. Materials and Methods

2.1. Materials

Preparation of $CaCO_3$ Particles: calcium chloride ($CaCl_2$) 99.9%, sodium carbonate (Na_2CO_3) 99.9%, sodium bicarbonate ($NaHCO_3$) 99.9%, poly(styrene sulfonate) sodium salt (PSS) 97%, ethylene glycol 98%, ethanol AR, and dextrane sulphate 95% were purchased from Sigma Aldrich. Milli-Q water with a resistance greater than 18.2 MΩ cm−1 was used for all experiments. *Bacterial panel*: Nunc White opaque 96-well microtiter plates (30396) were purchased from SPL Life Sciences Co., Ltd. (Gyeonggi-do, Korea (11192)). Lennox Broth (LB) (DF0402-17-0) was purchased from Becton Dickinson & Co., BD Diagnostic Systems, (Sparks MD, United States). Ampicillin sodium salt (BP1760-25) was purchased from Fisher BioReagents (Pittsburgh, Pennsylvania, United States). *SEM microscopy*: Polylysine-L (P4832: Mw 150,000-300,000, 0.01%, sterile-filtered, BioReagent, suitable for cell culture) and Glutaraldehyde (G7526: Grade I, 8% in H_2O, specially purified for use as an electron microscopy fixative or other sophisticated use) were purchased from Sigma-Aldrich (Merck group) (St. Louis, Missouri, United States). *Fluorescence microscopy*: Propidium Iodide 95% (PI) (440300250) was purchased from Acros Organics (Fair Lawn, New Jersey, United States). Deionized water (DW) was obtained by mechanical filtering through a Treion TS1173 column. All stock solutions were prepared and stored according to the instructions of the manufacturers.

2.2. Equipment

Incubator (Binder (Bohemia, NY, United States)), and rotary thermo-shaker MaxQ 4450 (Thermo scientific (Marietta, OH, United States)) were used to grow the bacterial panel. Ultrospec 2100 pro spectrometer (Amersham Bioscience (Cambridge, United Kingdom)) was used to measure absorbance to adjust the optical density of the bacterial panel culture. SynergyHTX multi-mode reader (BioTek Instruments Inc., Winooski, VT, United States) was used to measure the bioluminescent signal of the bacterial panel. High-resolution microscope Gemini SEM 300 from Zeiss (Carl-Zeiss-Strasse 22, Oberkochen, Germany), Q150T Turbo-Pumped Sputter of Palladium - Gold Coater (Quorom Technologies Pvt. Ltd., East Sussex, UK), and Helios 5UC system from Thermo Scientific ((Marietta, OH, United States)) were used for the SEM characterization of the vaterite particles. The scanning electron microscope (HRSEM-Jeol 7800, Jeol Ltd., Tokyo, Japan), and critical point dryer (K850 Critical Point Dryer, Quorom Technologies Ltd., East Sussex, UK) were used for the SEM characterization of the bacterial cells. Leica SP8 laser scanning microscope (Leica, Wetzlar, Germany), equipped with a solid-state laser with 552 nm light, HC PL APO CS2 63x/1.2 water immersion objective (Leica, Wetzlar, Germany), and Leica Application Suite X software (LASX, Leica, Wetzlar, Germany) were used for the fluorescence microscopy characterization.

2.3. Preparation of $CaCO_3$ Particles

The $CaCO_3$ particles in different shapes and sizes (toroids, ellipsoids, and spheroids) were synthesized by a conventional sustainable approach [66-68], based on coprecipitation of calcium chloride and sodium carbonate/hydrogen carbonate at different ratios in ethylene glycol medium [36]. The salts, $CaCl_2$ and $Na_2CO_3/NaHCO_3$ are dissolved in 1M ethylene glycol:H_2O in volumetric ratio of 85:15 mixture at selected concentrations (0.005M or 0.025M) for all the reactions to the final volume V = 40 mL (spheroids (0.025M $CaCl_2$ and 0.005M Na_2CO_3); ellipsoids (0.005M $CaCl_2$ and 0.025M Na_2CO_3); toroids (0.0025M $CaCl_2$ and 0.005M Na_2CO_3 + an organic additive 0.5 mg/mL poly(styrene sulfonate) (PSS)). Then, 20 mL $CaCl_2$ and 20 mL Na_2CO_3 were mixed under magnetic stirring at 400 rpm for 24 h at room temperature. Afterward, the particles were washed with DIW and twice with ethanol by centrifugation (5 krpm for 2 min). The yielded $CaCO_3$ particles were dispersed in ethanol to prevent recrystallization. An X-ray diffraction analysis (XRD) is presented in **Figure 1**, which

was conducted to validate the stability of the resulted $CaCO_3$ particles in the bacterial and LB medium solutions. The characteristic peaks remain the same for all three scenarios, verifying that the vaterite particles did not undergo a phase transition to calcite.

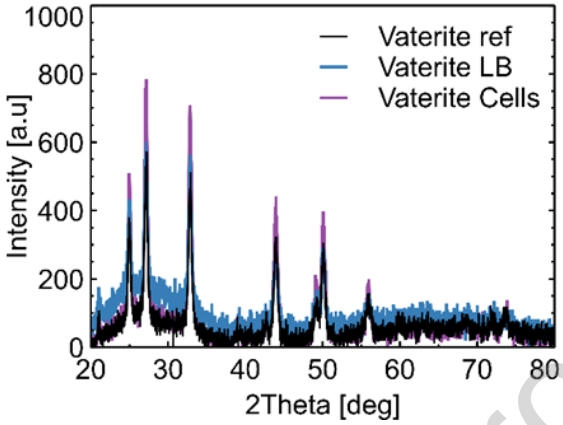

Figure 1. Preparation of $CaCO_3$ Particles. X-ray diffraction analysis (XRD) was conducted to validate the stability of the resulted $CaCO_3$ particles in the bacterial ('Vaterite Cells') and LB medium ('Vaterite LB') solutions, while only $CaCO_3$ particles were used as control ('Vaterite ref').

2.4. Bacterial panel

Different *E. coli* strains were used (**Table 1**), including DPD2794, TV1061 (obtained from Shimshon Belkin (Hebrew University, Jerusalem, Israel)), and K806NR (obtained from Jan Davies (University of Calgary, Calgary, Canada)). These strains contain a multi-copy plasmid (mcp) of plasmid-borne promoter fusion to the lux CDABE reporter operon. This lux operon contains 5 genes that are responsible for the synthesis of luciferase and its substrate tetradecanal [55]. Each of the strains consists of a different promoter as follows *recA* (DPD2794), *grpE* (TV1061), and *lasI* (K802NR). The translation of the plasmid is determined by the specific promoter. Therefore, according to the different promoter fusions the bacterial strains are sensitive to different types of stressors, including DNA-repair mechanisms such as DNA degradation and cross-link mutations (*recA*) [69, 70], metabolic changes such as cytotoxic substances (*grpE*) [71, 72], and bacterial communication as part of a positive feedback loop of *N*-3-oxo-dodecanoyl homoserine lactone ($3OC_{12}$-HSL) that is used for quorum sensing (*lasI*) [73, 74].

Table 1. The bioluminescent bioreporter bacterial panel.

Mode of Action	Sensitivity	Bacterial Strain	Promoter	lux Fusion Location	Ref.
Genotoxicity	DNA-Damage	DPD2794	*recA::lux*	mcp	[69, 70]
Cytotoxicity	Heat-Shock	TV1061	*grpE::lux*	mcp	[71, 72]
Quorum Sensing	$3OC_{12}$-HSL	K802NR	*lasI::lux*	mcp	[73, 74]

* multi-copy plasmid (mcp); *N*-3-oxo-dodecanoyl homoserine lactone ($3OC_{12}$-HSL)

2.5. Bacteria growing conditions

Firstly, the bacterial cells were grown on LB-agar plates from a strain stock with 20% (v/v) glycerol as a cell cryoprotectant additive that is stored at -80°C. The LB-agar plates (10g/L Tryptone; $5\ g/L$ Yeast Extract; 5 g/L NaCl) also contain 100 µg/mL ampicillin. After placing the cells on the plates, they were incubated for two days at *37°C* in an incubator. After, the bacterial strains were grown in a *10 mL* Lennox broth (LB) with 100 µg/mL ampicillin overnight at 37°C on a rotary thermo-shaker at *120 rpm* [75]. Then, the bacterial cultures were diluted to approximately 10^7 cell/mL (*100 µL* of the inoculum was transferred into *10 mL* of fresh medium) and regrown in the same medium without antibiotics at *26 °C* without shaking to the early exponential phase ($OD_{600\ nm}$ = 0.2) as determined by a spectrometer.

2.6. Scanning electron microscopy (SEM) characterization

The $CaCO_3$ particles were characterized by SEM. After the particles were dispersed in ethanol, they were then dropped (*5 µL*) onto indium tin oxide (ITO) glass or n-doped silicon substrate and dried for a few minutes. The dried particles were coated by sputtering with several nanometers of gold-palladium film. Quanta 200 FEG SEM was used to obtain images of the synthesized particles. A backscattered electron mode was used with an acceleration voltage of 5 kV at 0°C and under the pressure of 7.81 × 10−7 mbar. In addition, prior to the SEM characterization, the fixation and dehydration of the bacteria cells were done on a sample disc glass. After an early exponential phase was reached (grown as

explained in **section 2.5**), *1 mL* of the bacterial culture was centrifuged for *2 min* at *10 krpm* and the supernatant was removed, then the bacteria cells were rinsed two times with double-distilled water (DDW). After, *40 µL* of DDW was added to the bacteria cells pellet. The vaterite nanoparticles were added into the bacteria culture solution (the initial concentration is 5 mg/mL) at the tested dilutions of 1/10, 1/100, 1/1K, 1/10K, 1/10M, and 1/10B. In parallel, 40 µL of ready-made commercial *0.01%* polylysine-L solution was placed onto a glass disc and left for dehydration for over 1 hour at room temperature. Then, the polylysine-L residues were removed, and the glass discs were dried. After, *3 µL* of the bacteria solution with the vaterite particles were incubated on the glass disc for 1 hour at room temperature, which was then rinsed by DDW. Afterwards, *50 µL* of 4% (v/v) glutaraldehyde solution diluted in DDW was incubated on the glass discs for 1 hour. Then, the glass discs were rinsed three times for 10 minutes each with DDW under slow shaking. The bacteria cells were dehydrated by washing the glass discs in increasing concentrations of ethanol, as follow: two times in *10% (v/v)* for 10 minutes, two times in 20% (v/v) for 10 minutes, two times in 50% (v/v) for 10 minutes, two times in 70% (v/v) for 10 minutes, two times in 90% (v/v) for 10 minutes, two times in 95% (v/v) for 10 minutes, and four times in 100% (v/v) for 10 minutes. After, the glass discs were further dried in a critical point dryer. Lastly, the dried bacteria sample was coated and characterized by SEM, and images were captured at an accelerating voltage of 3kV.

2.7. Fluorescence microscopy characterization

The bacteria cells (grown as explained in **section 2.5**) were incubated with the vaterite nanoparticles (the initial concentration is 5 mg/mL) at different dilutions of 1/10, 1/100, 1/1K, 1/10K, 1/10M, and 1/10B. The red fluorescing propidium iodide (PI) which is a nucleic acid stain was used to indicate cell death. The bacterial cell solution with the vaterite particles was mixed with PI in a ratio of 80:10:10 µL, respectively. The samples were incubated in the dark at room temperature for 15 minutes. Then, 5 µL of stained bacteria suspensions were placed between a slide and 18 mm^2 coverslips. Leica SP8 laser scanning microscope was used for image acquisition, equipped with a solid-state laser with 552 nm light. The PI red emission signals were detected with a HyD (hybrid) detector in ranges of 580–650 nm.

2.8. Bioluminescence assay

A high-throughput approach was used to examine the bacterial panel responses in 96-well white opaque microtiter plates. The bacteria culture (grown as described in **section 2.5**) was mixed with the vaterite particles in different shapes and sizes (toroids, ellipsoids, and spheroids) in a *90 µL to 10 µL* ratio, respectively (n = 3 for each tested sample). A total of six particle types were tested, including toroids *0.5-1 µm*; toroids *15-25 µm*; ellipsoids *0.5-1.2 µm*; spheroids *0.5-1.2 µm*; spheroids *2-3 µm*; spheroids *5-7 µm*. The particles were tested in six dilutions (the initial concentration is 5 mg/mL), including 1/10, 1/100, 1/1K, 1/10K, 1/10M, and 1/10B. A relatively wide range of several tested concentrations of the vaterite nanoparticles was chosen, because it is important from the analysis aspect of the whole-cell bacterial biosensor responses. The bioreporter bacterial strains are sensitive and can show various response patterns to different concentrations of the same material, such as induction or inhibition of the bioluminescence signal. Therefore, in order to accurately determine the response of the bacterial cells to the vaterite nanoparticles, it is important to test a significantly wide range of concentrations. PSS buffered solution was used to dilute the vaterite particles, which is useful in stabilizing the vaterite particles and preventing their transformation into calcite. Therefore, both PSS solution and the growth medium of LB were tested as control samples. The same PSS concentration was used for the nanoparticles dispersion and in the control measurements. A SynergyHTX multi-mode reader was used to measure the bioluminescence activity of the bacterial panel, and the temperature of the samples was maintained at *26°C*. Relative light units (RLU) represent the luminescence values.

2.9. Viability assay

The effect of the vaterite particles on bacterial growth was examined with a bacterial viability assay. After growing the bacteria in LB medium (as described in **section 2.5**), they were mixed with the six nanoparticle types, including toroids *0.5-1* and *15-25 µm*; ellipsoids *0.5-1.2 µm*; spheroids *0.5-1.2*, *2-3* and *5-7 µm*. In addition, the same six dilutions were tested (the initial concentration is 5 mg/mL), including 1/10, 1/100, 1/1K, 1/10K, 1/10M, and 1/10B. After bacterial growth in LB, *10 µL* of the vaterite particles solution was added to *90 µL* of the bacterial culture inside the 96-well plate. After mixing the bacteria cells with the vaterite nanoparticles, the bacterial growth was monitored over 10 hours. The two samples of PSS and LB only were used as the controls. The same PSS concentration was used for the nanoparticles dispersion and in the control measurements.

2.10. Reproducibility and statistical analysis

The bacterial panel responses are monitored by the bioluminescence signal that is reported as an induction factor (IF) and calculated as follows: IF = Bs/Bc, where Bs and Bc are the maximum bioluminescence signals (B) of the tested sample (s) and the control (c), respectively. The most stable bacterial growth and signal were seen in a testing period of 4 hours. A minimum of thirty separate and different setups (independent repeats) were tested for each parameter. In addition, a range of values was defined based on the results for optimized analysis of the toxicity mode of action. When 1 ≤ IF ≤ 1.3, it was determined as having no particular effect (.). The positive induction effect was categorized into 3 level types: 1.3 < IF ≤ 1.5 marked as level 1 (+); 1.5 < IF < 1.8 marked as level 2 (++), and IF ≥ 1.8 marked as level 3 (+++). The ranges of the IF values were also determined based on additional recent studies of the research group [57, 62-65, 76, 77].

3. Results and Discussion

3.1. Particles characterization

The SEM characterization was conducted on the differently shaped $CaCO_3$ vaterite particles, including toroids *0.5-1* and *15-25 µm*, ellipsoids *0.5-1.2 µm*, and spheroids *0.5-1.2, 2-3*, and 5-7 µm (**Figure 2**). In the cases of toroids (0.5-1 µm (**Figure 2 (a)**) and *15-25 µm* (**Figure 2 (b)**)), the vaterite particles formed several-steps kinetics (additional magnifications can be seen in **Figure 1S** in supplementary data). The Toroidal particle formation occurs in the presence of an organic polymer chelator. The calcium chelating group of sulfonate shields the ions restricting the spherical radial growth to a defined toroidal thickness related to the polymeric chain length. The smaller size toroids particles (*0.5-1 µm* (**Figure 2 (a)**)) demonstrated a rounded vaterite toroids form, while the bigger size toroids particles (*15-25 µm* (**Figure 2 (b)**)) demonstrated flat vaterite particles. In the case of ellipsoids (*0.5-1.2 µm* (**Figure 2 (c)**)), the aggregation of nano-seeds into ellipsoidal particles can be identified (additional magnifications can be seen in **Figure 2S** in supplementary data). This may be caused by an increment of their number and total surface energy [78], in our case, such surface charge control is applied by ion ration in the growth bath. There are several phases in the crystallization process [22]. In general, the first stage of crystallization is the amorphous phase, then nanoparticles are formed that later construct the big crystals of several hundreds of nanometres, the ration between ions creating vaterite. The presence of

more carbonate ions results in lower zeta potential and less negative surface charge. The phenomenon of changes in surface charge occurs due to the initial stage of crystallization and the creation of different amorphous phases, which are the result of kinetic rates of $CaCO_3$ resulting in different outer charge. Generally, a higher ratio of carbonate to calcium ions reduces the negatively charged surface. In addition, in the cases of spheroids (*0.5-1.2 μm* **Figure 2 (d)**, *2-3 μm* (**Figure 2 (e)**), and *5-7 μm* (**Figure 2 (f)**)), the self-assembled nanoscale crystals can be seen in a grain-based mesoporous structure (additional magnifications can be seen in **Figure 3S** in supplementary data) [8, 79]. The spherulite surface roughness is of the same order as the size of single monocrystals (~30 nm) and it is mostly dictated by the size of individual grains as well as leads to diffuse light scattering, and other attractive optical properties. Generally, the effect of surface roughness along with geometrical properties of refractive index can for example generate a resonant scattering [8, 80, 81].

The SEM characterization was also conducted on a mixture of the bacteria cells with the various $CaCO_3$ vaterite particles (size of 0.5 μm, and three different geometries) (**Figure 3**). The structure of the *E. coli* cells is clearly identified with their standard morphology [82], while the particles might have washed away during the fixation process of the cells (additional magnifications can be seen in **Figure 4S** in supplementary data). For example, SEM characterization was previously used to examine calcified bacteria cells within vaterite particles [83]. Visual effects on the morphology of the bacterial cells were not observed. Thus, it is an indication that the tested vaterite particles did not integrate with the bacterial cell wall. The results of the SEM characterization are strengthened by the SEM images of differently shaped $CaCO_3$ particles in the literature [11], as well as specifically with the findings of *H. Barhom et al.* that investigated the same particles [36]. It was reported that the specific surface area is the lowest in spheroids (40.6 m^2/g) as compared to those of ellipsoids (43.1 m^2/g) and toroids (75.5 m^2/g). This can also affect the enhanced adsorption capacity of the toroids particles. The addition of the organic additive poly(styrene sulfonate) (PSS) that can locate on the particles surface may explain the increased surface area of the toroidal particles and may also contribute to their porosity. Moreover, the average pore size of the toroidal particles (*3.57 nm*) is lower than those of spheroidal and ellipsoidal particles (*12.7 and 15.7 nm*, respectively), which can be explained by the filling of pores by PSS. As a result, the pore volume of the differently shaped particles also varies (ellipsoids (0.172 cm^3/g), spheroids (0.127 cm^3/g), and toroids (0.084 cm^3/g)). In addition, PSS is negatively charged and thus contributes to the more negative zeta-potential of the toroidal particles (−12 mV), compared to those of spheroids and ellipsoids *(−2 and −0.8 mV*). To conclude,

the SEM characterization demonstrated the expected sizes and shapes of the various vaterite particles.

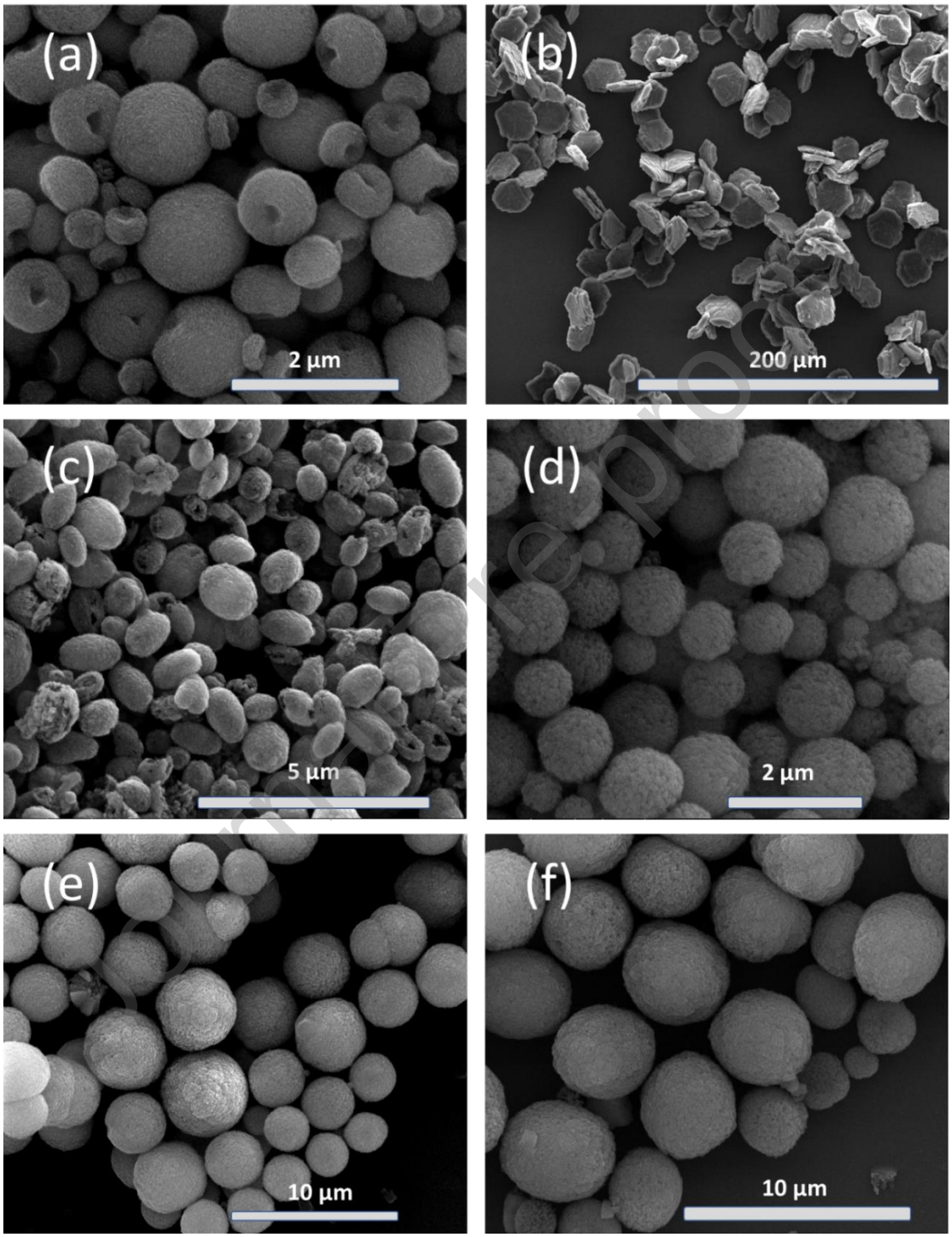

Figure 2. SEM images of vaterite particles. (a, b) Toroidal particles in the sizes of *0.5-1 µm* and *15-25 µm* respectively (c) Ellipsoids *0.5-1.2 µm*; (d, e, f) Spheroids *0.5-1.2 µm*; Spheroids *2-3 µm*; Spheroids *5-7 µm* in average sizes, statistical processing was performed by image analysis.

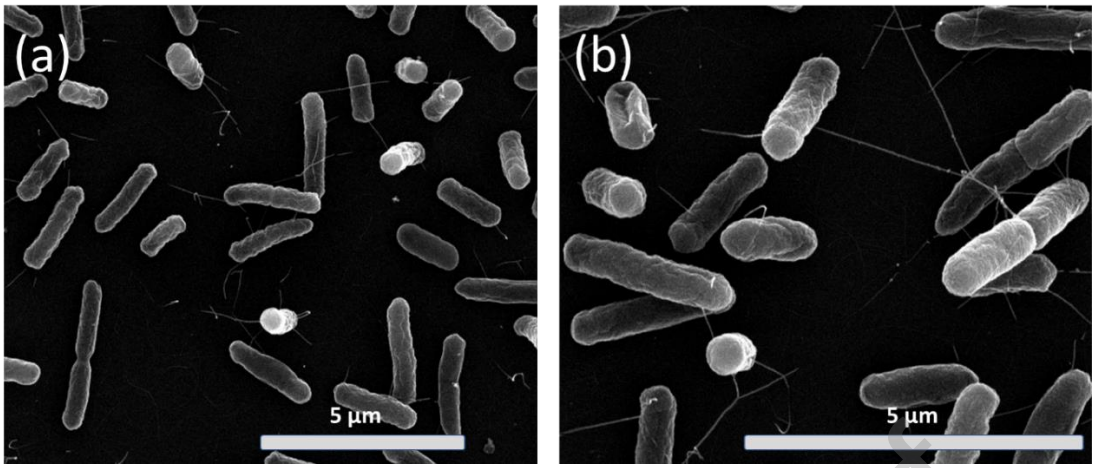

Figure 3. SEM characterization of bacteria cells exposed to vaterite particles. The SEM characterization was conducted on a mixture of the bacteria cells with the various $CaCO_3$ vaterite particles (size of 0.5 µm, and three different geometries). The structure of the *Escherichia coli* (*E. coli*) cells ((a) and (b)) is clearly identified with their standard morphology, while the particles might have washed away during the fixation process of the cells.

3.2. Fluorescence imaging of the bacterial cells

The fluorescence microscopy characterization was also conducted on the differently shaped $CaCO_3$ vaterite particles, including toroids *0.5-1* and *15-25 µm*, ellipsoids *0.5-1.2 µm*, and spheroids *0.5-1.2*, *2-3, and 5-7 µm* (**Figure 4**). For example, confocal fluorescence images were previously used to characterize *E. coli* cells that were incorporated into vaterite crystals [84]. In this study, the bacteria cells were grown and then incubated with the vaterite particles at different dilutions of 1/10, 1/100, 1/1K, 1/10K, 1/10M, and 1/10B. Then, a red fluorescing nucleic acid stain, propidium iodide (PI), was used to indicate cell death. PI is a DNA intercalator because of its positive charge that attaches to the bacteria DNA; thus, it only stains cells with damaged cytoplasmic membranes [85]. Therefore, PI allows to identify between bacteria with intact and damaged cytoplasmic membranes and is commonly used to indicate cell death [86]. In addition, PI has NH_2 groups and thus can form hydrogen bonds, combining that with its charge it may enable the PI binding capabilities to proteins and nanomaterials [87].

Generally, effects on the bacterial cells were seen only in the highest tested concentration of the vaterite particles (1/10) (**Figure 4**). While, in all the rest of the tested dilutions, no difference was seen from the control (**Figure 5S** in supplementary data). Among all the

tested particles, toroids *15-25 µm* showed the strongest antibacterial effect and aggregates. Smaller aggregates and bacterial cells dyed in red (indicative of cell death) were also seen in all the tested sizes of spheroids, including *0.5-1.2, 2-3, and 5-7 µm*. While bacterial cells dyed in red without visible aggregates were seen in the cases of toroids *0.5-1 µm* and ellipsoids *0.5-1.2 µm*. The differences seen between the results of the particles might also be explained by the findings of *H. Barhom et al.* [36]. For example, it was reported that in the case of ellipsoidal particles, the contact angle between the particles and the cell membrane is lower than for spheroidal and toroidal particles. In addition, previous studies investigated the survival of bacteria cells within $CaCO_3$ particles [88]. For example, fluorescence microscopy with green fluorescence by SYTO was utilized to depict total cells, and it was reported that the viability of the cells was affected by the carbon source in such that $NaHCO_3$ results in higher viability than CO_2 supplementation [89]. Also, it was concluded that the survival of bacteria cells within $CaCO_3$ particles is dependent on the bacterial species and decreased with time [90]. To conclude, bacterial cell death and aggregates were seen only in the highest tested concentration of the vaterite particles (1/10), where it was most visible in the case of toroids *15-25 µm*.

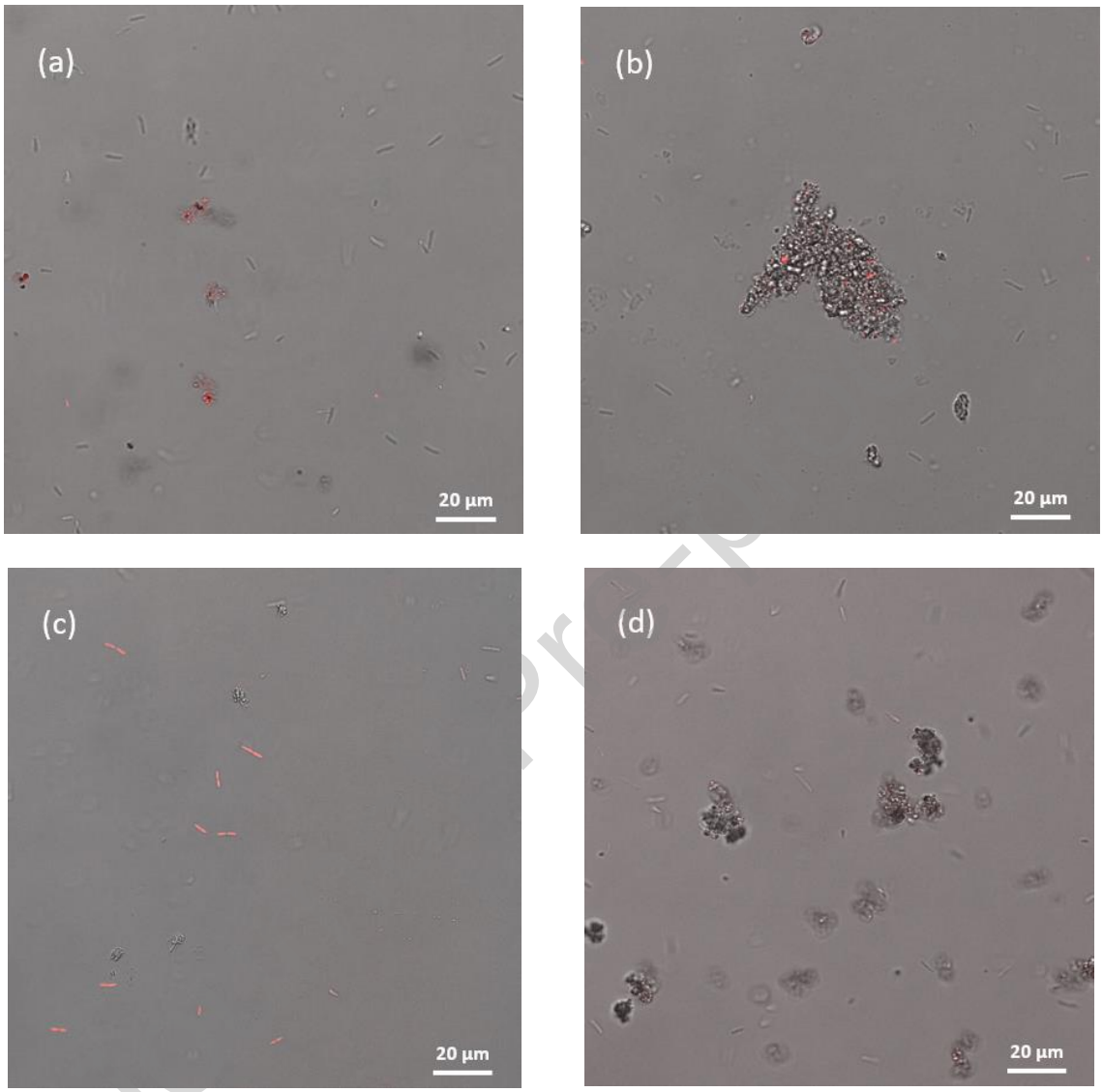
(a)
20 µm
(b)
20 µm
(c)
20 µm
(d)
20 µm

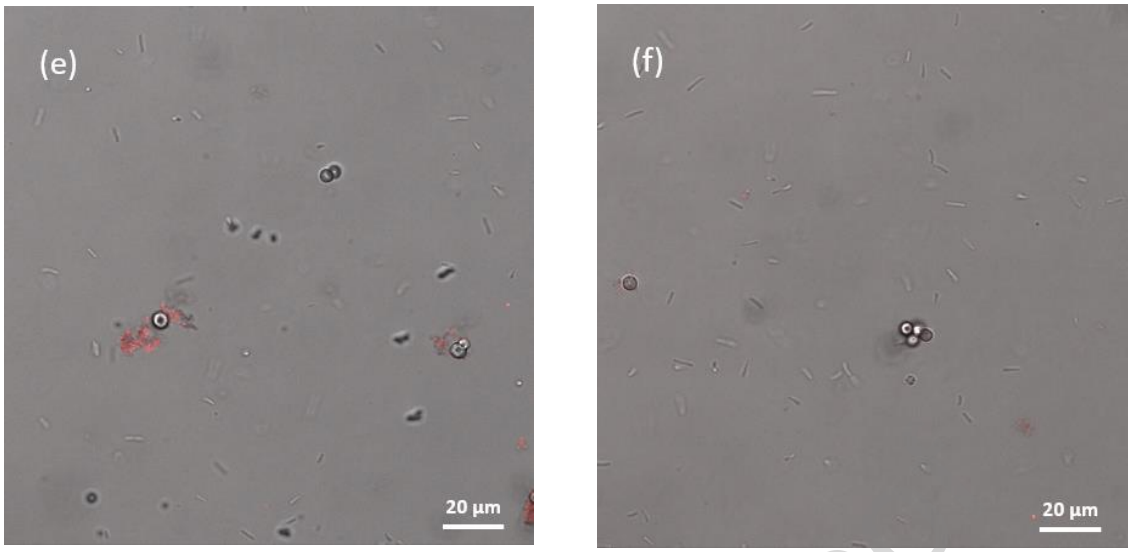

Figure 4. Fluorescence microscopy characterization. The highest tested concentration of 1/10 dilution: (a) Toroids *0.5-1 µm*; (b) Toroids *15-25 µm*; (c) Ellipsoids *0.5-1.2 µm*; (d) Spheroids *0.5-1.2 µm*; (e) Spheroids *2-3 µm*; (f) Spheroids *5-7 µm*.

3.3. Biocompatibility estimated by bacterial mode-of action

The bioluminescent bacterial panel is based on bacterial cells that are genetically modified to produce light in the presence of specific chemicals. Three different *E. coli* strains were tested that are sensitive to different types of stressors, including cytotoxicity (TV1061), genotoxicity (DPD2794), and quorum-sensing stress (K802NR). A light signal change is generated after the exposure of the bioluminescent bacterial panel to the tested vaterite particles. This signal shift reflects the toxicity mode-of-action of the particles. All six vaterite particle types were tested, including toroids *0.5-1* and *15-25 µm*, ellipsoids *0.5-1.2 µm*, and spheroids *0.5-1.2, 2-3, and 5-7 µm*. The particles were tested in six dilutions (the initial concentration is 5 mg/mL), including 1/10, 1/100, 1/1K, 1/10K, 1/10M, and 1/10B (**Figure 5**, **Table 2**, and **Table 1S** in supplementary data). The results are reported as induction factor (IF) which is calculated as the light signal ratio relative to the control. Therefore, an IF = 1 means that the response of the bacteria strain produced a light signal that is equivalent to the control, whereas an IF > 1 means an induction effect, and IF < 1 means an inhibition effect. Generally, all the tested vaterite particles resulted in an induction effect (IF > 1) on the bacterial panel (**Figure 5**). Whilst the PSS showed IF values similar to the control (IF ~ 1.1).

In addition, the results indicate that the bacterial panel responses were significantly higher after exposure to the toroids (1.557 ≤ IF ≤ 2.271) and ellipsoids particles (1.712 ≤ IF ≤ 2.018), as compared to the spheroids particles (1.134 ≤ IF ≤ 1.494) (**Table 1S** in

supplementary data). Also, all the tested bacterial strains showed a clear induction effect after exposure to both toroids and ellipsoids particles (**Table 2**). This indicates that the tested toroids and ellipsoids particles have multiple toxicity mode-of-action on the bacterial panel, including metabolic changes such as with cytotoxic substances (TV1061) (**Figure 5A**) [71, 72], DNA-repair mechanisms such as DNA degradation and cross-link mutations (DPD2794) (**Figure 5B**) [69, 70], and bacterial communication as part of a positive feedback loop of *N*-3-oxo-dodecanoyl homoserine lactone ($3OC_{12}$-HSL) that is used for quorum sensing (K802NR) (**Figure 5C**) [73, 74]. Also, it is possible to identify that there is an effect of the vaterite particle size on the induction of the bacterial cytotoxic effect (TV1061). Toroids vaterite particles of smaller sizes (*0.5-1 μm*) resulted in a higher induction response (+++), which was observed only in the cytotoxic sensitive strains (**Table 2**). Moreover, dose-dependent patterns in decreasing concentrations (increasing dilutions) were not seen in both cases of toroids and ellipsoids particles, as the IF values were mainly between 1.8 to 2.0. Whilst, in the cases of spheroids particles, clearer dose-dependent patterns were identified where lower concentrations (higher dilutions) resulted in lower IF values, mainly identified in the smallest tested spheroids size of *0.5-1.2 μm* (**Figure 5**). The biggest tested spheroids size of *5-7 μm* resulted in only a mild induction effect with a stable IF value of ~ 1.4.

The biocompatibility of vaterite particles was thoroughly tested in previous studies [17, 48]. The cytotoxicity of vaterite particles was not identified when tested with human ovarian carcinoma cells ES2 and human fibroblasts MRC5 [16], osteoblast cell line (MG-63) [49], human gastric carcinoma cells (SGC-7901) [50], normal cells (HEK 293T cells) [51], normal human dermal fibroblasts (NHDF) [52], and primary human T-lymphocytes [53]. Moreover, a recent study examined the biological toxicological profile of $CaCO_3$ particles in cell lines (a mouse embryonic fibroblast cell line (NIH 3T3) and a human breast adenocarcinoma cell line (MCF7)), and *in vivo* on zebrafish (*Danio Rerio*), and concluded that no cytotoxicity or genotoxicity was identified [54]. Prior information was not found on quorum sensing influences of $CaCO_3$ particles. Moreover, another point for discussion is the optical features of the tested vaterite particles. In the bioluminescence assay in this study, only emission was detected without initial excitation. However, a possible effect is that the light signal emitted by the bacteria cells may be scattered by vaterite [8], which can later result in a higher total RLU value. However, the particle size influence may reject this possibility, because it was identified that there is an effect of the toroids vaterite particles size on the induction of the bacterial cytotoxic effect (TV1061). To conclude, the vaterite particles resulted in an induction effect (IF > 1) on the bacterial panel, which was significantly higher after exposure to the toroids ($1.557 \leq IF \leq 2.271$) and ellipsoids particles ($1.712 \leq IF \leq 2.018$), as compared to the spheroids particles ($1.134 \leq IF \leq 1.494$), in all the tested bacterial strains.

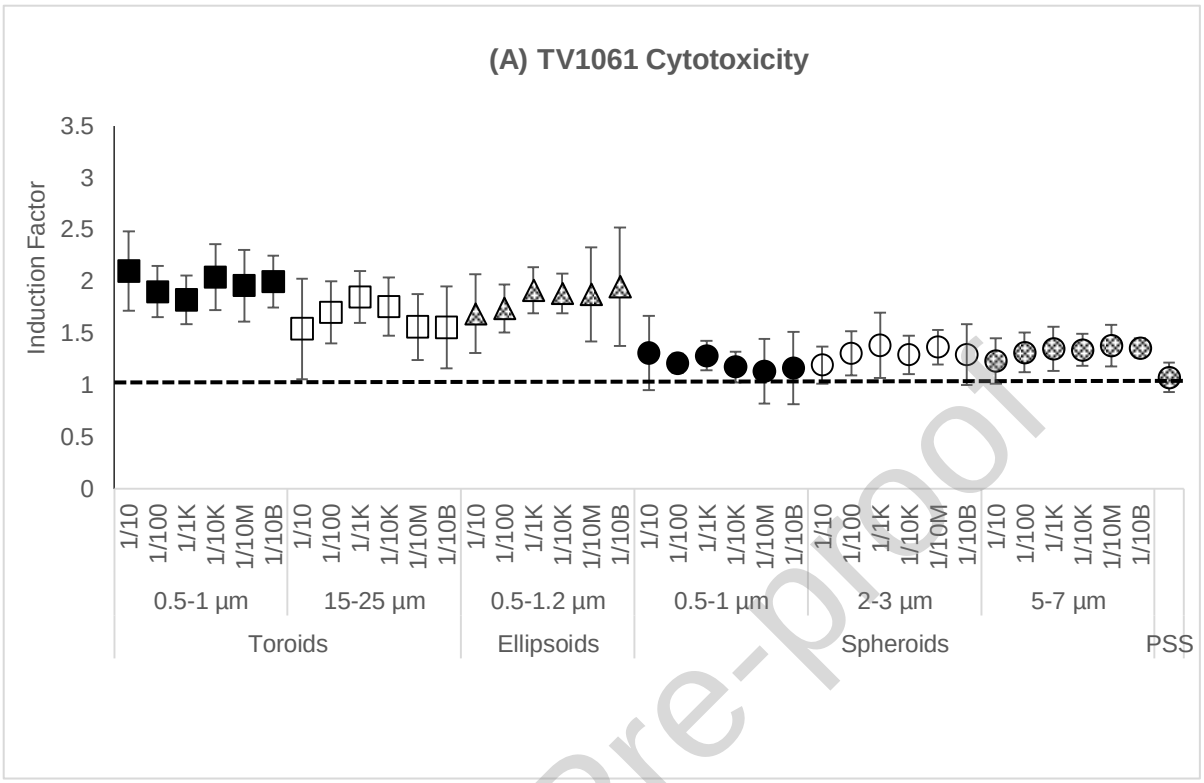

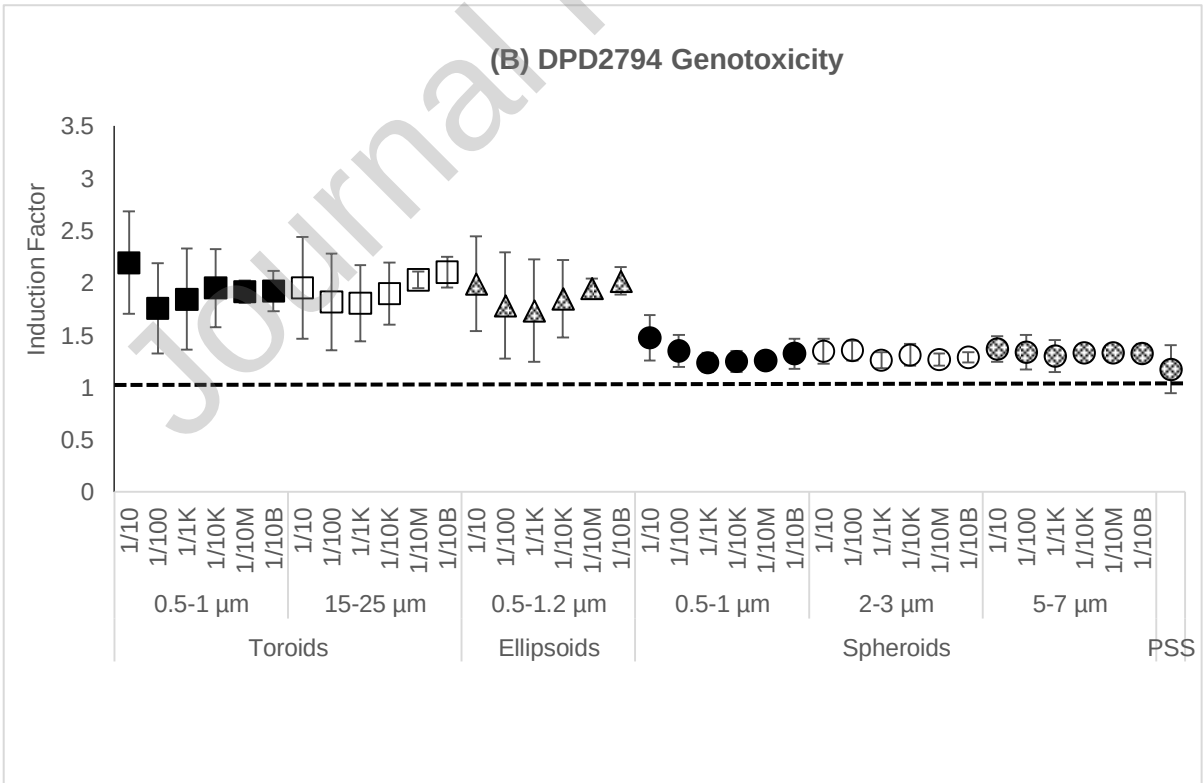

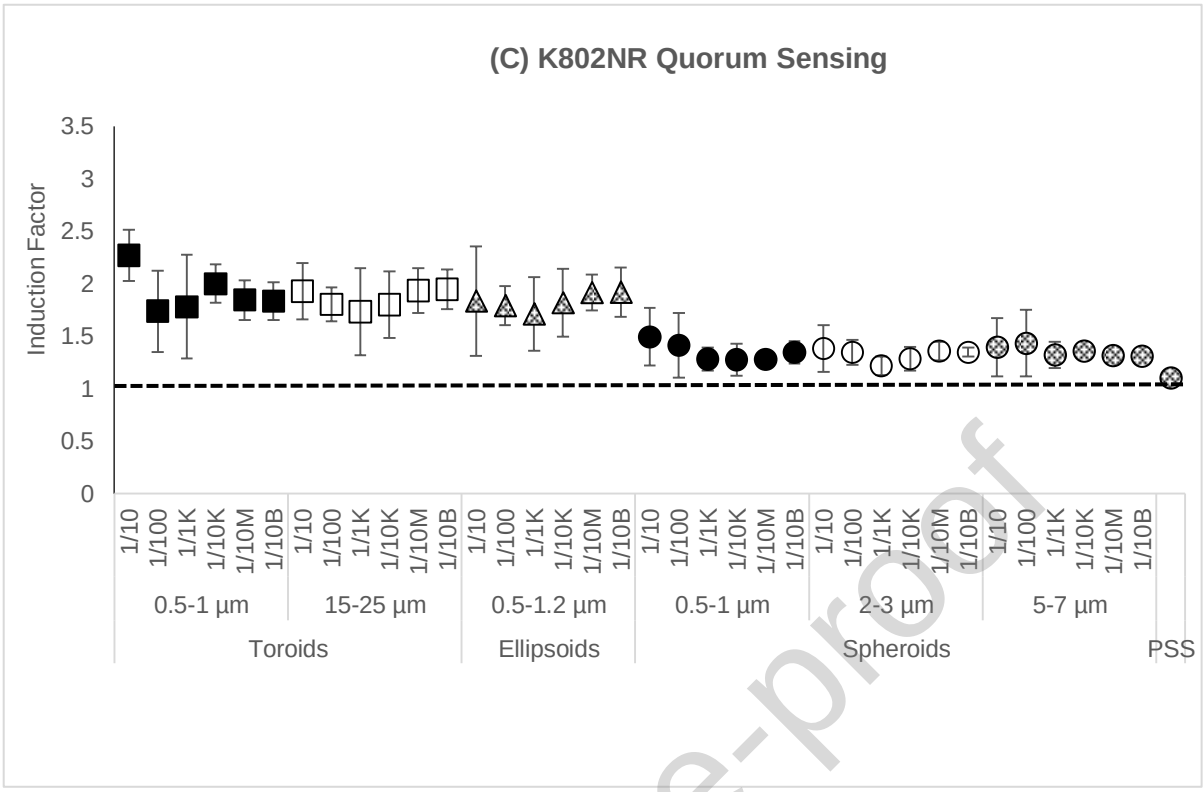

Figure 5. Bioluminescence assay. The bacterial panel responses are monitored by the bioluminescence signal that is reported as induction factor (IF) and calculated as follows: IF = Bs/Bc, where Bs and Bc are the maximum bioluminescence signals (B) of the tested sample (s) and the control (c), respectively. PSS (Poly(Styrene Sulfonate)). The initial concentration of the vaterite particles is 5 mg/mL.

Table 2. Induction and inhibition effects in the bioluminescence assay.

Vaterite Particles			Bacterial Strains		
Shape	**Size**	**Dilution**	**TV1061**	**DPD2794**	**K802NR**
Toroids	**0.5-1 μm**	**1/10**	**+++**	**+++**	**+++**
		1/100	**+++**	++	++
		1/1K	**+++**	**+++**	++
		1/10K	**+++**	**+++**	**+++**
		1/10M	**+++**	**+++**	**+++**
		1/10B	**+++**	**+++**	**+++**
	15-25 μm	**1/10**	++	**+++**	**+++**
		1/100	++	**+++**	**+++**
		1/1K	**+++**	**+++**	++
		1/10K	++	**+++**	**+++**
		1/10M	++	**+++**	**+++**
		1/10B	++	**+++**	**+++**
Ellipsoids	**0.5-1.2 μm**	**1/10**	++	**+++**	**+++**
		1/100	++	++	++
		1/1K	**+++**	++	++
		1/10K	**+++**	**+++**	**+++**
		1/10M	**+++**	**+++**	**+++**
		1/10B	**+++**	**+++**	**+++**
Spheroids	**0.5-1 μm**	**1/10**	+	+	+
		1/100	.	+	+
		1/1K	.	.	.
		1/10K	.	.	.
		1/10M	.	.	.
		1/10B	.	+	+
	2-3 μm	**1/10**	.	+	+
		1/100	+	+	+
		1/1K	+	.	.
		1/10K	.	+	.
		1/10M	+	.	+
		1/10B	.	.	+
	5-7 μm	**1/10**	.	+	+
		1/100	+	+	+
		1/1K	+	+	+
		1/10K	+	+	+
		1/10M	+	+	+
		1/10B	+	+	+
PSS			.	.	.

* Based on the results, a range of values was defined for optimized analysis of the toxicity mode of action. When 1 ≤ IF ≤ 1.3, it was determined as having no particular effect (.). The positive induction effect was categorized into 3 level types: 1.3 < IF ≤ 1.5 marked as level 1 (+); 1.5 < IF < 1.8 marked as level 2 (++), and IF ≥ 1.8 marked as level 3 (+++). The initial concentration of the vaterite particles is 5 mg/mL.

3.4. Viability assay

The viability of the bacteria strains was also examined after exposure to the various vaterite particles. All six vaterite particle types were tested, including toroids *0.5-1* and *15-25 µm*, ellipsoids *0.5-1.2 µm*, and spheroids *0.5-1.2, 2-3, and 5-7 µm*. The particles were tested in four dilutions (the initial concentration is 5 mg/mL), including 1/10, 1/100, 1/1K, and 1/10K (**Figure 6**). In addition, a negative control (only LB growth medium) and a PSS sample were also tested. Generally, the vaterite particles did not affect the viability of the bacterial cells. The bacterial growth is characterized by a starting value of 0.1 ($OD_{600\,nm}$) in the lag stage, reaching a value of 0.2 ($OD_{600\,nm}$) in the log stage in the time period of *2-4 hours*, which continues to mildly increase with time in the stationary stage. Among the tested dilutions of the differently shaped particles, only the highest tested concentration (1/10 dilution) showed an influence on the viability of the bacterial cells in some particles, including toroids *15-25 µm*, and spheroids *0.5-1.2, 2-3, and 5-7 µm*. The influence that was seen in these cases is an increase in the OD_{600nm} values throughout the bacterial growth curve. Whilst still the normal bacterial growth curve was identified in these cases, with the lag, log, and stationary growth stages. The last death (decline) stage was not identified within the 10 hours testing period.

A possible explanation for the increased $OD_{600\,nm}$ values in the highest concentration only in the following four particle types of toroids *15-25 µm*, and spheroids *0.5-1.2, 2-3*, and *5-7 µm*, can be the effect of these particles on the spectrophotometer absorbance measurement, and not necessarily on the viability of the bacterial cells. The effect is induced by the vaterite light scattering property, resulting in lower transmission of the beam. The latter fact is consistent with a characteristic family of optical modes that are supported in vaterite particles with similar diameters [8]. The particles in the mixture can also create sediment, and due to its high concentration to reduce the transmitted signal and interrupt the reading of the spectrophotometer. These results are strengthened by the findings of previous studies, which reported that no influence was found of vaterite particles on cell viability [16, 17, 49-52, 54]. While it was even found to be enhanced [8]. Specifically, *H. Barhom et al.* also examined the viability influence of the same tested differently shaped vaterite particles (spheroids, ellipsoids, and toroids) on C6 glioma cell model, and the particles displayed the absence of cytotoxicity even at the highest cell-to-particle ratio [36]. To conclude, the vaterite particles did not affect the viability of the bacterial cells, and the death stage was not identified within the *10 hours* testing period.

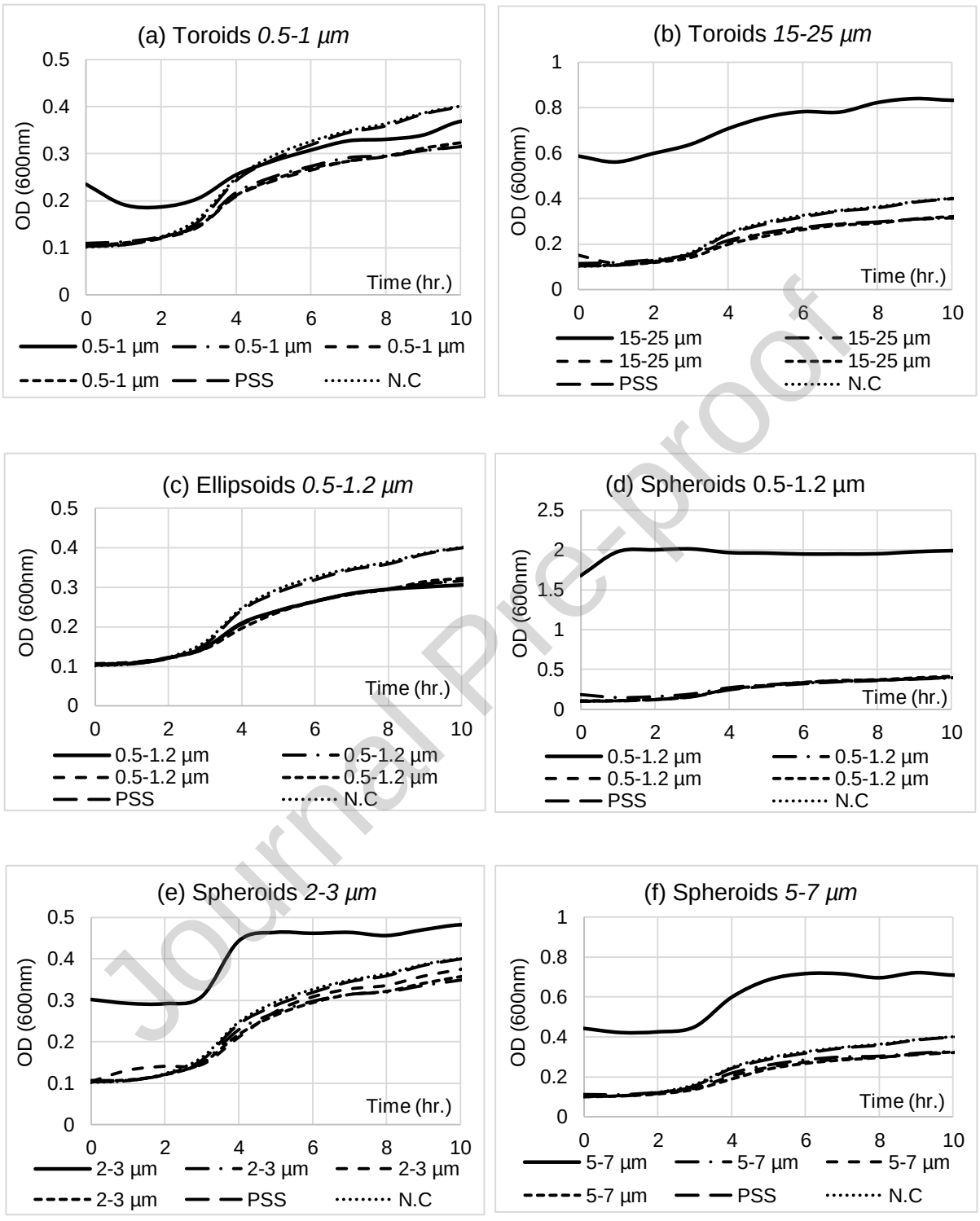

Figure 6. Viability assay. (a) Toroids *0.5-1 μm*; (b) Toroids *15-25 μm*; (c) Ellipsoids *0.5-1.2 μm*; (d) Spheroids *0.5-1.2 μm*; (e) Spheroids *2-3 μm*; (f) Spheroids *5-7 μm*. PSS (Poly(Styrene Sulfonate)); N.C. (Negative Control). The initial concentration of the vaterite particles is 5 mg/mL. Normal bacterial growth curves were identified, with the lag, log, and

stationary growth stages. Only the highest tested concentration (1/10 dilution) showed some influence, in cases of toroids *15-25 µm*, and spheroids *0.5-1.2, 2-3, and 5-7 µm*.

4. Conclusions

The biocompatibility of differently shaped $CaCO_3$ vaterite particles (toroids, ellipsoids, and spheroids) were estimated by bacterial toxicity mode-of-action with a whole-cell biosensor. The bioluminescent bacterial panel is based on three different *E. coli* strains that are sensitive to general stresses, i.e., cytotoxicity (TV1061), genotoxicity (DPD2794), and quorum-sensing stress (K802NR). Firstly, both SEM and fluorescence microscopy characterizations were conducted. The SEM characterization demonstrated the expected sizes and shapes of the various vaterite particles. Also, the structure of the *E. coli* cells was clearly identified with their standard morphology. In the fluorescence microscopy characterization, bacterial cell death and aggregates were seen only in the highest tested concentration of the vaterite particles (1/10), where it was most visible in the case of toroids *15-25 µm.* After, bioluminescence and viability assays were performed. By exposing the bioluminescent bacterial panel to the vaterite particles, a light signal change is then generated, reflecting the toxicity mode-of-action of the particles. The vaterite particles resulted in an induction effect (IF > 1) on the bacterial panel, which were significantly higher after exposure to the toroids (1.557 ≤ IF ≤ 2.271) and ellipsoids particles (1.712 ≤ IF ≤ 2.018), as compared to the spheroids particles (1.134 ≤ IF ≤ 1.494), in all the tested bacterial strains. This indicates that the tested toroids and ellipsoids particles have multiple toxicity mode-of-action on the bacterial panel. In addition, the vaterite particles did not affect the viability of the bacterial cells, and the death stage was not identified within the 10 hours testing period. The bacterial monitoring demonstrated the biofriendly nature of especially spheroids vaterite nanoparticles. Bacterial monitoring results in identifying specific signatures that will allow accurate detection of the toxicity mode-of-action.

Supplementary Data: The data on the full SEM and fluorescence microscopy characterization results is available in the supplementary data file.

Author Contributions: Evgeni Eltzov: Conceptualization, Methodology, Resources, Writing - review & editing, Supervision, Project administration, Funding acquisition. **Pavel Ginzburg**: Conceptualization, Methodology, Resources, Writing - review & editing, Supervision, Project administration, Funding acquisition. **Dorin Harpaz**: Validation, Data curation, Writing -

original draft. **Boris Veltman**: Investigation, Validation. **Hani Barhom**: Investigation, Validation. All authors have read and agreed to the published version of the manuscript.

Acknowledgments: The authors thank Dr. Zahava Barkay and Vered Hodenberg for their help with the SEM processing and image measurements.

Conflicts of Interest: The authors declared no potential conflicts of interest concerning the research, authorship, and/or publication of this article.

Data Availability: The datasets generated during and/or analyzed during the current study are available from the corresponding author on reasonable request.

References

[1] A. S. Timin, D. J. Gould, and G. B. Sukhorukov, "Multi-layer microcapsules: Fresh insights and new applications," *Expert opinion on drug delivery,* vol. 14, no. 5, pp. 583-587, 2017, doi: https://doi.org/10.1080/17425247.2017.1285279.

[2] M. V. Zyuzin, A. S. Timin, and G. B. Sukhorukov, "Multilayer capsules inside biological systems: State-of-the-art and open challenges," *Langmuir,* vol. 35, no. 13, pp. 4747-4762, 2019, doi: https://doi.org/10.1021/acs.langmuir.8b04280.

[3] M. Humar, S. J. J. Kwok, M. Choi, A. K. Yetisen, S. Cho, and S.-H. Yun, "Toward biomaterial-based implantable photonic devices," *Nanophotonics,* vol. 6, no. 2, pp. 414-434, 2017, doi: https://doi.org/10.1515/nanoph-2016-0003.

[4] B. Pelaz *et al.*, "Diverse Applications of Nanomedicine. ACS nano 11, 2313–2381," ed, 2017.

[5] K. Zarschler *et al.*, "Ultrasmall inorganic nanoparticles: State-of-the-art and perspectives for biomedical applications," *Nanomedicine: Nanotechnology, Biology and Medicine,* vol. 12, no. 6, pp. 1663-1701, 2016, doi: https://doi.org/10.1016/j.nano.2016.02.019.

[6] O. Braissant, E. P. Verrecchia, and M. Aragno, "Is the contribution of bacteria to terrestrial carbon budget greatly underestimated?," *Naturwissenschaften,* vol. 89, no. 8, pp. 366-370, 2002, doi: https://doi.org/10.1007/s00114-002-0340-0.

[7] R. Riding, "Microbial carbonates: the geological record of calcified bacterial–algal mats and biofilms," *Sedimentology,* vol. 47, pp. 179-214, 2000, doi: https://doi.org/10.1046/j.1365-3091.2000.00003.x.

[8] H. Barhom *et al.*, "Biological Kerker effect boosts light collection efficiency in plants," *Nano letters,* vol. 19, no. 10, pp. 7062-7071, 2019, doi: https://doi.org/10.1021/acs.nanolett.9b02540.

[9] C. Dupraz, R. P. Reid, O. Braissant, A. W. Decho, R. S. Norman, and P. T. Visscher, "Processes of carbonate precipitation in modern microbial mats," *Earth-Science Reviews,* vol. 96, no. 3, pp. 141-162, 2009/10/01/ 2009, doi: https://doi.org/10.1016/j.earscirev.2008.10.005.

[10] R. E. Martinez, E. Gardés, O. S. Pokrovsky, J. Schott, and E. H. Oelkers, "Do photosynthetic bacteria have a protective mechanism against carbonate precipitation at their surfaces?," *Geochimica et Cosmochimica Acta,* vol. 74, no. 4, pp. 1329-1337, 2010/02/15/ 2010, doi: https://doi.org/10.1016/j.gca.2009.11.025.

[11] Y. Boyjoo, V. K. Pareek, and J. Liu, "Synthesis of micro and nano-sized calcium carbonate particles and their applications," *Journal of Materials Chemistry A,* vol. 2, no. 35, pp. 14270-14288, 2014, doi: https://doi.org/10.1039/C4TA02070G.

[12] A. R. Rastinehad *et al.*, "Gold nanoshell-localized photothermal ablation of prostate tumors in a clinical pilot device study," *Proceedings of the National Academy of Sciences,* vol. 116, no. 37, pp. 18590-18596, 2019, doi: https://doi.org/10.1073/pnas.1906929116.

[13] R. E. Noskov *et al.*, "Golden Vaterite as a Mesoscopic Metamaterial for Biophotonic Applications," *Advanced Materials,* p. 2008484, 2021, doi: https://doi.org/10.1002/adma.202008484.

[14] K. Seidensaal, S. B. Harrabi, and J. Debus, "Molecular Imaging for Particle Therapy: Current Approach and Future Directions," in *Molecular Imaging in Oncology*: Springer, 2020, pp. 865-879.

[15] D. V. Volodkin, A. I. Petrov, M. Prevot, and G. B. Sukhorukov, "Matrix polyelectrolyte microcapsules: new system for macromolecule encapsulation," *Langmuir,* vol. 20, no. 8, pp. 3398-3406, 2004, doi: https://doi.org/10.1021/la036177z.

[16] B. V. Parakhonskiy *et al.*, "Tailored intracellular delivery via a crystal phase transition in 400 nm vaterite particles," *Biomaterials Science,* vol. 1, no. 12, pp. 1273-1281, 2013, doi: https://doi.org/10.1039/C3BM60141B.

[17] Y. I. Svenskaya, A. M. Pavlov, D. A. Gorin, D. J. Gould, B. V. Parakhonskiy, and G. B. Sukhorukov, "Photodynamic therapy platform based on localized delivery of photosensitizer by vaterite submicron particles," *Colloids and Surfaces B: Biointerfaces,* vol. 146, pp. 171-179, 2016, doi: https://doi.org/10.1016/j.colsurfb.2016.05.090.

[18] Q. Dong, J. Li, L. Cui, H. Jian, A. Wang, and S. Bai, "Using porous CaCO3/hyaluronic acid nanocages to accommodate hydrophobic photosensitizer in aqueous media for photodynamic therapy," *Colloids and Surfaces A: Physicochemical and Engineering Aspects,* vol. 516, pp. 190-198, 2017, doi: https://doi.org/10.1016/j.colsurfa.2016.12.027.

[19] Y. I. Svenskaya *et al.*, "A simple non-invasive approach toward efficient transdermal drug delivery based on biodegradable particulate system," *ACS applied materials & interfaces,* vol. 11, no. 19, pp. 17270-17282, 2019, doi: https://doi.org/10.1021/acsami.9b04305.

[20] Y. I. Svenskaya *et al.*, "Enhanced topical psoralen–ultraviolet A therapy via targeting to hair follicles," *British Journal of Dermatology,* vol. 182, no. 6, pp. 1479-1481, 2020, doi: https://doi.org/10.1111/bjd.18800.

[21] D. B. Trushina, T. V. Bukreeva, M. V. Kovalchuk, and M. N. Antipina, "CaCO3 vaterite microparticles for biomedical and personal care applications," *Materials Science and Engineering: C,* vol. 45, pp. 644-658, 2014, doi: https://doi.org/10.1016/j.msec.2014.04.050.

[22] H. Bahrom *et al.*, "Controllable synthesis of calcium carbonate with different geometry: comprehensive analysis of particles formation, their cellular uptake and biocompatibility," *arXiv preprint arXiv:2106.15974,* 2021, doi: https://doi.org/10.48550/arXiv.2106.15974.

[23] R. E. Noskov, I. I. Shishkin, H. Barhom, and P. Ginzburg, "Non-Mie optical resonances in anisotropic biomineral nanoparticles," *Nanoscale,* vol. 10, no. 45, pp. 21031-21040, 2018, doi: https://doi.org/10.1039/C8NR07561A.

[24] O. Cherkas, T. Beuvier, D. W. Breiby, Y. Chushkin, F. Zontone, and A. Gibaud, "Direct observation of microparticle porosity changes in solid-state vaterite to calcite transformation by coherent X-ray diffraction imaging," *Crystal Growth & Design,* vol. 17, no. 8, pp. 4183-4188, 2017, doi: https://doi.org/10.1021/acs.cgd.7b00476.

[25] C. Rodriguez-Navarro, C. Jimenez-Lopez, A. Rodriguez-Navarro, M. T. Gonzalez-Muñoz, and M. Rodriguez-Gallego, "Bacterially mediated mineralization of vaterite," *Geochimica et Cosmochimica Acta,* vol. 71, no. 5, pp. 1197-1213, 2007, doi: https://doi.org/10.1016/j.gca.2006.11.031.

[26] A. Hall and J. D. Taylor, "The occurrence of vaterite in gastropod egg-shells," *Mineralogical Magazine,* vol. 38, no. 296, pp. 521-522, 1971, doi: https://doi.org/10.1180/minmag.1971.038.296.17.

[27] L. Qiao, Q.-L. Feng, and Z. Li, "Special vaterite found in freshwater lackluster pearls," *Crystal growth & design,* vol. 7, no. 2, pp. 275-279, 2007, doi: https://doi.org/10.1021/cg060309f.

[28] D. J. Sutor and S. E. Wooley, "Gallstone of unusual composition: calcite, aragonite, and vaterite," *Science,* vol. 159, no. 3819, pp. 1113-1114, 1968, doi: https://doi.org/10.1126/science.159.3819.1113

[29] N. A. Palchik and T. N. Moroz, "Polymorph modifications of calcium carbonate in gallstones," *Journal of crystal growth,* vol. 283, no. 3-4, pp. 450-456, 2005, doi: https://doi.org/10.1016/j.jcrysgro.2005.05.035.

[30] J. Kanakis, P. Malkaj, J. Petroheilos, and E. Dalas, "The crystallization of calcium carbonate on porcine and human cardiac valves and the antimineralization effect of sodium alginate," *Journal of Crystal Growth,* vol. 223, no. 4, pp. 557-564, 2001, doi: https://doi.org/10.1016/S0022-0248(01)00698-4.

[31] R. Lakshminarayanan, E. O. Chi-Jin, X. J. Loh, R. M. Kini, and S. Valiyaveettil, "Purification and Characterization of a Vaterite-Inducing Peptide, Pelovaterin, from the Eggshells of Pelodiscus s Inensis (Chinese Soft-Shelled Turtle)," *Biomacromolecules,* vol. 6, no. 3, pp. 1429-1437, 2005, doi: https://doi.org/10.1021/bm049276f.

[32] A. P. Ariani, K. J. Wittmann, and E. Franco, "A comparative study of static bodies in mysid crustaceans: evolutionary implications of crystallographic characteristics," *The Biological Bulletin,* vol. 185, no. 3, pp. 393-404, 1993, doi: https://doi.org/10.2307/1542480.

[33] G. Falini, S. Fermani, S. Vanzo, M. Miletic, and G. Zaffino, "Influence on the formation of aragonite or vaterite by otolith macromolecules," *European Journal of Inorganic Chemistry,* vol. 2005, no. 1, pp. 162-167, 2005, doi: https://doi.org/10.1002/ejic.200400419.

[34] S. Mann, *Biomineralization: principles and concepts in bioinorganic materials chemistry*. Oxford University Press on Demand, 2001.

[35] A. G. Christy, "A review of the structures of vaterite: the impossible, the possible, and the likely," *Crystal Growth & Design,* vol. 17, no. 6, pp. 3567-3578, 2017, doi: https://doi.org/10.1021/acs.cgd.7b00481.

[36] H. Bahrom *et al.*, "Controllable synthesis of calcium carbonate with different geometry: Comprehensive analysis of particle formation, cellular uptake, and biocompatibility," *ACS Sustainable Chemistry & Engineering,* vol. 7, no. 23, pp. 19142-19156, 2019, doi: https://doi.org/https://doi.org/10.48550/arXiv.2106.15974

[37] G. Falini, S. Fermani, M. Gazzano, and A. Ripamonti, "Polymorphism and architectural crystal assembly of calcium carbonate in biologically inspired polymeric matrices," *Journal of the Chemical Society, Dalton Transactions,* no. 21, pp. 3983-3987, 2000, doi: https://doi.org/10.1039/B003334K.

[38] K. Naka and Y. Chujo, "Control of crystal nucleation and growth of calcium carbonate by synthetic substrates," *Chemistry of materials,* vol. 13, no. 10, pp. 3245-3259, 2001, doi: https://doi.org/10.1021/cm011035g.

[39] P. Malkaj and E. Dalas, "Calcium carbonate crystallization in the presence of aspartic acid," *Crystal growth & design,* vol. 4, no. 4, pp. 721-723, 2004, doi: https://doi.org/10.1021/cg030014r.

[40] K. Sawada, "The mechanisms of crystallization and transformation of calcium carbonates," *Pure and Applied Chemistry,* vol. 69, no. 5, pp. 921-928, 1997, doi: https://doi.org/10.1351/pac199769050921.

[41] A. Jada and A. Verraes, "Preparation and microelectrophoresis characterisation of calcium carbonate particles in the presence of anionic polyelectrolyte," *Colloids and Surfaces A: Physicochemical and Engineering Aspects,* vol. 219, no. 1, pp. 7-15, 2003/06/19/ 2003, doi: https://doi.org/10.1016/S0927-7757(03)00010-4.

[42] O. Braissant, G. Cailleau, C. Dupraz, and E. P. Verrecchia, "Bacterially induced mineralization of calcium carbonate in terrestrial environments: the role of exopolysaccharides and amino acids," *Journal of Sedimentary Research,* vol. 73, no. 3, pp. 485-490, 2003, doi: https://doi.org/10.1306/111302730485.

[43] F. Manoli, J. Kanakis, P. Malkaj, and E. Dalas, "The effect of aminoacids on the crystal growth of calcium carbonate," *Journal of Crystal Growth,* vol. 236, no. 1, pp. 363-370, 2002/03/01/ 2002, doi: https://doi.org/10.1016/S0022-0248(01)02164-9.

[44] A.-J. Xie, Y.-H. Shen, C.-Y. Zhang, Z.-W. Yuan, X.-M. Zhu, and Y.-M. Yang, "Crystal growth of calcium carbonate with various morphologies in different amino acid systems," *Journal of Crystal Growth,* vol. 285, no. 3, pp. 436-443, 2005/12/01/ 2005, doi: https://doi.org/10.1016/j.jcrysgro.2005.08.039.

[45] Q. Shen *et al.*, "Crystallization and Aggregation Behaviors of Calcium Carbonate in the Presence of Poly(vinylpyrrolidone) and Sodium Dodecyl Sulfate," *The Journal of Physical Chemistry B,* vol. 109, no. 39, pp. 18342-18347, 2005/10/01 2005, doi: https://doi.org/10.1021/jp052094a

[46] K. B. Chekroun, C. Rodríguez-Navarro, M. T. González-Muñoz, J. M. Arias, G. Cultrone, and M. Rodríguez-Gallego, "Precipitation and growth morphology of calcium carbonate induced by Myxococcus xanthus: implications for recognition of bacterial carbonates," *Journal of Sedimentary Research,* vol. 74, no. 6, pp. 868-876, 2004, doi: https://doi.org/10.1306/050504740868.

[47] H. Barhum, T. Alon, M. Attrash, A. Machnev, I. Shishkin, and P. Ginzburg, "Multicolor Phenylenediamine Carbon Dots for Metal-Ion Detection with Picomolar Sensitivity," *ACS Applied Nano Materials,* vol. 4, no. 9, pp. 9919-9931, 2021/09/24 2021, doi: https://doi.org/10.1021/acsanm.1c02496

[48] R. A. Verkhovskii, O. V. Nechaeva, O. I. Guslyakova, and Y. I. Svenskaya, "Dark cytotoxicity of submicrometer vaterite particles loaded with photosensitizer Fotoditazin and the vaterite-based core–shells structures," *Reviews on Clinical Pharmacology and Drug Therapy,* vol. 19, no. 3, pp. 333-338, 2021, doi: https://doi.org/10.17816/RCF193333-338.

[49] R. Schröder *et al.*, "Particles of vaterite, a metastable CaCO3 polymorph, exhibit high biocompatibility for human osteoblasts and endothelial cells and may serve as a biomaterial for rapid bone regeneration," *Journal of tissue engineering and regenerative medicine,* vol. 12, no. 7, pp. 1754-1768, 2018, doi: https://doi.org/10.1002/term.2703.

[50] L.-H. Fu, Y.-Y. Dong, M.-G. Ma, S.-M. Li, and R.-C. Sun, "Compare study CaCO3 crystals on the cellulose substrate by microwave-assisted method and ultrasound agitation method," *Ultrasonics sonochemistry,* vol. 20, no. 3, pp. 839-845, 2013, doi: https://doi.org/10.1016/j.ultsonch.2012.11.001.

[51] J. Tang *et al.*, "One-Step Bulk Preparation of Calcium Carbonate Nanotubes and Its Application in Anticancer Drug Delivery," *Biological Trace Element Research,* vol. 147, no. 1, pp. 408-417, 2012/06/01 2012, doi: https://doi.org/10.1007/s12011-012-9325-9.

[52] M. S. Savelyeva *et al.*, "Vaterite coatings on electrospun polymeric fibers for biomedical applications," *Journal of Biomedical Materials Research Part A,* vol. 105, no. 1, pp. 94-103, 2017, doi: https://doi.org/10.1002/jbm.a.35870.

[53] Y. Tarakanchikova *et al.*, "A highly efficient and safe gene delivery platform based on polyelectrolyte core–shell nanoparticles for hard-to-transfect clinically relevant cell types," *Journal of Materials Chemistry B,* vol. 8, no. 41, pp. 9576-9588, 2020, doi: https://doi.org/10.1039/D0TB01359E.

[54] M. d'Amora, F. Liendo, F. A. Deorsola, S. Bensaid, and S. Giordani, "Toxicological profile of calcium carbonate nanoparticles for industrial applications," *Colloids and Surfaces B: Biointerfaces,* vol. 190, p. 110947, 2020, doi: https://doi.org/10.1016/j.colsurfb.2020.110947.

[55] E. Eltzov, A. Cohen, and R. S. Marks, "Bioluminescent liquid light guide pad biosensor for indoor air toxicity monitoring," *Analytical chemistry,* vol. 87, no. 7, pp. 3655-3661, 2015, doi: https://doi.org/10.1021/ac5038208.

[56] E. Eltzov, V. Pavluchkov, M. Burstin, and R. S. Marks, "Creation of a fiber optic based biosensor for air toxicity monitoring," *Sensors and Actuators B: Chemical,* vol. 155, no. 2, pp. 859-867, 2011, doi: https://doi.org/10.1016/j.snb.2011.01.062.

[57] B. Veltman, D. Harpaz, S. Melamed, Z. Tietel, L. Tsror, and E. Eltzov, "Whole-cell bacterial biosensor for volatile detection from Pectobacterium-infected potatoes enables early identification of potato tuber soft rot disease," *Talanta,* vol. 247, p. 123545, 2022/09/01/ 2022, doi: https://doi.org/10.1016/j.talanta.2022.123545.

[58] A. Bakhrat, E. Eltzov, Y. Finkelstein, R. S. Marks, and D. Raveh, "UV and arsenate toxicity: a specific and sensitive yeast bioluminescence assay," *Cell Biology and Toxicology,* vol. 27, no. 3, pp. 227-236, 2011, doi: https://doi.org/10.1007/s10565-011-9184-8.

[59] K. Hakkila, T. Green, P. Leskinen, A. Ivask, R. Marks, and M. Virta, "Detection of bioavailable heavy metals in EILATox-Oregon samples using whole-cell luminescent bacterial sensors in suspension or immobilized onto fibre-optic tips," *Journal of Applied Toxicology,* vol. 24, no. 5, pp. 333-342, 2004/09/01 2004, doi: https://doi.org/10.1002/jat.1020.

[60] E. Eltzov, A. Yehuda, and R. S. Marks, "Creation of a new portable biosensor for water toxicity determination," *Sensors and Actuators B: Chemical,* vol. 221, pp. 1044-1054, 2015/12/31/ 2015, doi: https://doi.org/10.1016/j.snb.2015.06.153.

[61] E. Eltzov, D. Z. Ben-Yosef, A. Kushmaro, and R. Marks, "Detection of sub-inhibitory antibiotic concentrations via luminescent sensing bacteria and prediction of their mode of action," *Sensors and Actuators B: Chemical,* vol. 129, no. 2, pp. 685-692, 2008/02/22/ 2008, doi: https://doi.org/10.1016/j.snb.2007.09.054.

[62] D. Harpaz *et al.*, "Measuring Artificial Sweeteners Toxicity Using a Bioluminescent Bacterial Panel," *Molecules,* vol. 23, no. 10, 2018, doi: https://doi.org/10.3390/molecules23102454

[63] T. Axelrod, E. Eltzov, M. Lerman, D. Harpaz, and R. S. Marks, "Cigarette smoke toxicity modes of action estimated by a bioluminescent bioreporter bacterial panel," *Talanta,* vol. 226, p. 122076, 2021/05/01/ 2021, doi: https://doi.org/10.1016/j.talanta.2020.122076.

[64] D. Harpaz, B. Veltman, Y. Sadeh, R. S. Marks, N. Bernstein, and E. Eltzov, "The effect of cannabis toxicity on a model microbiome bacterium epitomized by a panel of bioluminescent E. coli," *Chemosphere,* vol. 263, p. 128241, 2021/01/01/ 2021, doi: https://doi.org/10.1016/j.chemosphere.2020.128241.

[65] D. Harpaz, B. Veltman, D. Katz, and E. Eltzov, "Whole-cell bacterial biosensor with the capability to detect red palm weevil, Rhynchophorus ferrugineus, in date palm trees, Phoenix dactylifera: a proof of concept study," *Journal of Biotechnology,* vol. 357, pp. 47-55, 2022/09/20/ 2022, doi: https://doi.org/10.1016/j.jbiotec.2022.08.007.

[66] D. B. Trushina, S. N. Sulyanov, T. V. Bukreeva, and M. V. Kovalchuk, "Size control and structure features of spherical calcium carbonate particles," *Crystallography reports,* vol. 60, no. 4, pp. 570-577, 2015, doi: https://doi.org/10.1134/S1063774515040227.

[67] B. Parakhonskiy *et al.*, "The influence of the size and aspect ratio of anisotropic, porous CaCO 3 particles on their uptake by cells," *Journal of nanobiotechnology,* vol. 13, no. 1, pp. 1-13, 2015, doi: https://doi.org/10.1186/s12951-015-0111-7.

[68] M. V. Novoselova *et al.*, "Submicron-sized nanocomposite magnetic-sensitive carriers: controllable organ distribution and biological effects," *Polymers,* vol. 11, no. 6, p. 1082, 2019, doi: https://doi.org/10.3390/polym11061082.

[69] S. I. Feinstein, Y. Chemajovsky, L. Chen, L. Maroteaux, and Y. Mory, "Expression of human interferon genes using the recA promoter of Escherichia coli," *Nucleic Acids Research,* vol. 11, no. 9, pp. 2927-2941, 1983, doi: https://doi.org/10.1093/nar/11.9.2927.

[70] M. B. Gu, J. Min, and R. A. LaRossa, "Bacterial bioluminescent emission from recombinant Escherichia coli harboring a recA::luxCDABE fusion," *Journal of Biochemical and Biophysical Methods,* vol. 45, no. 1, pp. 45-56, 2000/08/10/ 2000, doi: https://doi.org/10.1016/S0165-022X(00)00100-7.

[71] T. K. Van Dyk, T. R. Reed, A. C. Vollmer, and R. A. LaRossa, "Synergistic induction of the heat shock response in Escherichia coli by simultaneous treatment with chemical inducers," *Journal of bacteriology,* vol. 177, no. 20, pp. 6001-6004, 1995, doi: https://doi.org/10.1128/jb.177.20.6001-6004.1995.

[72] T. K. Van Dyk, W. R. Majarian, K. B. Konstantinov, R. M. Young, P. S. Dhurjati, and R. A. Larossa, "Rapid and sensitive pollutant detection by induction of heat shock gene-bioluminescence gene fusions," *Applied and environmental microbiology,* vol. 60, no. 5, pp. 1414-1420, 1994, doi: https://doi.org/10.1128/aem.60.5.1414-1420.1994.

[73] E.-B. Goh, G. Yim, W. Tsui, J. McClure, M. G. Surette, and J. Davies, "Transcriptional modulation of bacterial gene expression by subinhibitory concentrations of antibiotics," *Proceedings of the National Academy of Sciences,* vol. 99, no. 26, pp. 17025-17030, 2002, doi: https://doi.org/10.1073/pnas.252607699.

[74] D. M. Shlaes, J. H. Shlaes, J. Davies, and R. Williamson, "Escherichia coli susceptible to glycopeptide antibiotics," *Antimicrobial agents and chemotherapy,* vol. 33, no. 2, pp. 192-197, 1989, doi: https://doi.org/10.1128/AAC.33.2.192.

[75] J. H. Miller, "Experiments in Molecular Genetics," *Cold Spring Harbor Laboratory Press,* 1972.

[76] D. Chalupowicz, B. Veltman, S. Droby, and E. Eltzov, "Evaluating the use of biosensors for monitoring of Penicillium digitatum infection in citrus fruit," *Sensors and Actuators B: Chemical,* vol. 311, p. 127896, 2020/05/15/ 2020, doi: https://doi.org/10.1016/j.snb.2020.127896.

[77] J. Ma, B. Veltman, Z. Tietel, L. Tsror, Y. Liu, and E. Eltzov, "Monitoring of infection volatile markers using CMOS-based luminescent bioreporters," *Talanta,* vol. 219, p. 121333, 2020/11/01/ 2020, doi: https://doi.org/10.1016/j.talanta.2020.121333.

[78] Y. I. Svenskaya *et al.*, "Key parameters for size-and shape-controlled synthesis of vaterite particles," *Crystal Growth & Design,* vol. 18, no. 1, pp. 331-337, 2018, doi: https://doi.org/10.1021/acs.cgd.7b01328.

[79] S. J. Parkin *et al.*, "Highly birefringent vaterite microspheres: production, characterization and applications for optical micromanipulation," *Optics express,* vol. 17, no. 24, pp. 21944-21955, 2009, doi: https://doi.org/10.1364/OE.17.021944.

[80] C. Li, G. W. Kattawar, and P. Yang, "Effects of surface roughness on light scattering by small particles," *Journal of Quantitative Spectroscopy and Radiative Transfer,* vol. 89, no. 1, pp. 123-131, 2004/11/15/ 2004, doi: https://doi.org/10.1016/j.jqsrt.2004.05.016.

[81] G. Song, Y. Wang, and D. Q. Tan, "A review of surface roughness impact on dielectric film properties," *IET Nanodielectrics,* vol. 5, no. 1, pp. 1-23, 2022/03/01 2022, doi: https://doi.org/10.1049/nde2.12026.

[82] W.-R. Li, X.-B. Xie, Q.-S. Shi, H.-Y. Zeng, O. U. Y. You-Sheng, and Y.-B. Chen, "Antibacterial activity and mechanism of silver nanoparticles on Escherichia coli," *Applied microbiology and biotechnology,* vol. 85, no. 4, pp. 1115-1122, 2010, doi: https://doi.org/10.1007/s00253-009-2159-5.

[83] C. Rodriguez-Navarro, F. Jroundi, M. Schiro, E. Ruiz-Agudo, and M. T. González-Muñoz, "Influence of substrate mineralogy on bacterial mineralization of calcium carbonate: implications for stone conservation," *Applied and environmental microbiology,* vol. 78, no. 11, pp. 4017-4029, 2012, doi: https://doi.org/10.1128/AEM.07044-11.

[84] M. Zhang *et al.*, "Particle-attachment crystallization facilitates the occlusion of micrometer-sized Escherichia coli in calcium carbonate crystals with stable fluorescence," *Journal of Materials Chemistry B,* vol. 8, no. 40, pp. 9269-9276, 2020, doi: https://doi.org/10.1039/D0TB01978J.

[85] E. Eltzov and R. S. Marks, "Fiber-Optic Based Cell Sensors," in *Whole Cell Sensing Systems I: Reporter Cells and Devices*, S. Belkin and M. B. Gu Eds. Berlin, Heidelberg: Springer Berlin Heidelberg, 2010, pp. 131-154.

[86] E. Eltzov, R. S. Marks, S. Voost, B. A. Wullings, and M. B. Heringa, "Flow-through real time bacterial biosensor for toxic compounds in water," *Sensors and Actuators B: Chemical,* vol. 142, no. 1, pp. 11-18, 2009/10/12/ 2009, doi: https://doi.org/10.1016/j.snb.2009.08.024.

[87] B. Veltman, D. Harpaz, Y. Cohen, E. Poverenov, and E. Eltzov, "Characterization of the selective binding of modified chitosan nanoparticles to Gram-negative bacteria strains," *International Journal of Biological Macromolecules,* vol. 194, pp. 666-675, 2022/01/01/ 2022, doi: https://doi.org/10.1016/j.ijbiomac.2021.11.111.

[88] N. K. Dhami, A. Mukherjee, and M. S. Reddy, "Viability of calcifying bacterial formulations in fly ash for applications in building materials," *Journal of Industrial Microbiology and Biotechnology,* vol. 40, no. 12, pp. 1403-1413, 2013, doi: https://doi.org/10.1007/s10295-013-1338-7.

[89] N. K. Dhami, A. Mukherjee, and M. S. Reddy, "Micrographical, minerological and nano-mechanical characterisation of microbial carbonates from urease and carbonic anhydrase producing bacteria," *Ecological Engineering,* vol. 94, pp. 443-454, 2016, doi: https://doi.org/10.1016/j.ecoleng.2016.06.013.

[90] D. V. Zamarreño, R. Inkpen, and E. May, "Carbonate crystals precipitated by freshwater bacteria and their use as a limestone consolidant," *Applied and environmental microbiology,* vol. 75, no. 18, pp. 5981-5990, 2009, doi: https://doi.org/10.1128/AEM.02079-08.

Graphical Abstract

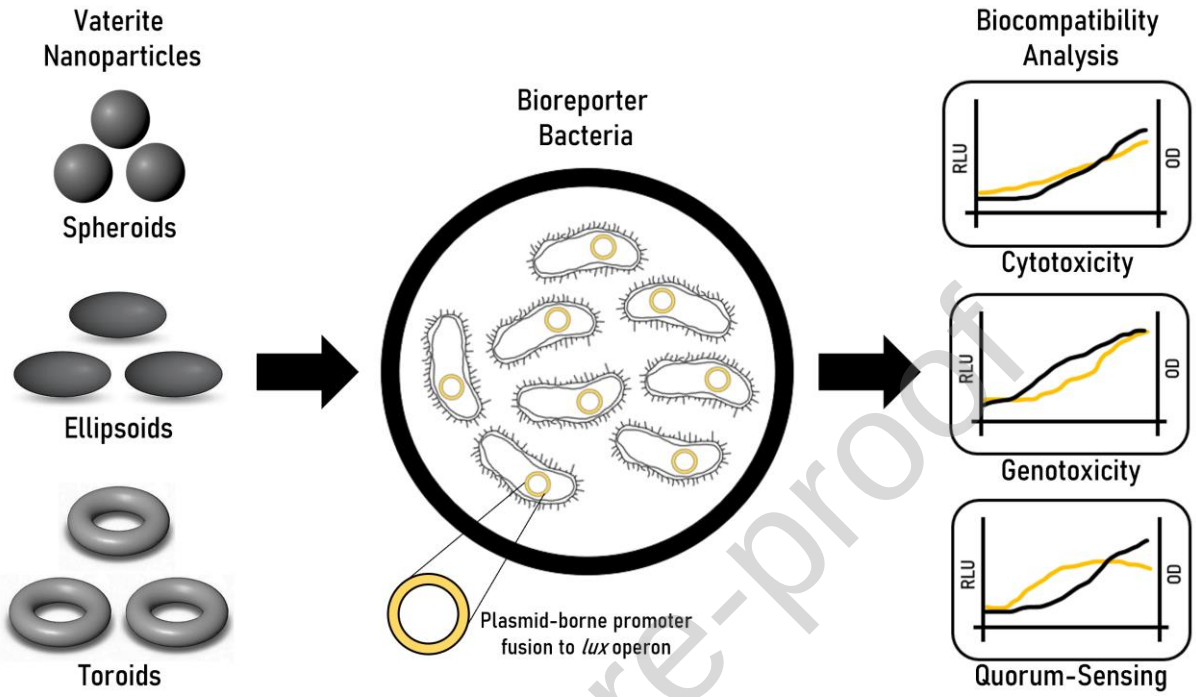

Author Contributions: Evgeni Eltzov: Conceptualization, Methodology, Resources, Writing - review & editing, Supervision, Project administration, Funding acquisition. **Pavel Ginzburg**: Conceptualization, Methodology, Resources, Writing - review & editing, Supervision, Project administration, Funding acquisition. **Dorin Harpaz**: Validation, Data curation, Writing - original draft. **Boris Veltman**: Investigation, Validation. **Hani Barhom**: Investigation, Validation. All authors have read and agreed to the published version of the manuscript.

Declaration of interests

☒ The authors declare that they have no known competing financial interests or personal relationships that could have appeared to influence the work reported in this paper.
☐The authors declare the following financial interests/personal relationships which may be considered as potential competing interests:

Highlights

- Biocompatibility of vaterite particles (toroids, ellipsoids, and spheroids)
- Bacterial panel sensitive to cytotoxicity, genotoxicity, and quorum-sensing
- Cell death and aggregates were observed only in the highest particles concentration
- Induction factor (IF > 1) after exposure to the toroids and ellipsoids particles
- Demonstrated the biofriendly nature of especially spheroids vaterite nanoparticles